Abdominal Radiology
https://doi.org/10.1007/s00261-024-04535-x

CASE REPORT

Pseudo-myometrial thinning in placental site trophoblastic tumors: a case series with multiparametric MRI

Takahiro Tsuboyama[1,2] · Takuya Fukuzawa[3] · Moto Nakaya[4] · Yasuchiyo Toyama[5] · Ayumi Ohya[3] · Katsuhiro Sano[4] · Akiko Takahata[5] · Kansuke Kido[2] · Noriyuki Tomiyama[2]

Received: 15 July 2024 / Revised: 14 August 2024 / Accepted: 15 August 2024

Abstract

Purpose Placental site trophoblastic tumor (PSTT) is a rare form of gestational trophoblastic neoplasm with few previous imaging case reports. We report multiparametric MRI findings in four cases of PSTT with special emphasis on the "pseudo-myometrial thinning" underlying the tumor.

Methods We reviewed multiparametric MRI and pathologic findings in four cases of PSTT from four institutions. Signal intensity, enhancement pattern, margins, and location of the tumors were evaluated, and myometrial thickness underlying the tumor and normal myometrial thickness contralateral to the tumor were measured on MRI. The myometrial thickness underlying the tumor was also measured in the resected specimen and compared with the myometrial thickness measured on MRI using the Friedman test.

Results All tumors showed heterogeneous signal intensity on T1-weighted imaging, T2-weighted imaging (T2WI), and diffusion-weighted imaging. Three of the four tumors had a hypervascular area on dynamic contrast-enhanced (DCE) MRI. A hypointense rim on T2WI and DCE-MRI was seen in all tumors. All tumors protruded into the uterine cavity to varying degrees and extended into the myometrium close to the serosa. The myometrial thickness underlying the tumor measured on MRI (median thickness, 1.2 mm) was significantly thinner than that measured on pathology (median thickness, 9.5 mm) and normal myometrial thickness contralateral to the tumor on MRI (median thickness, 10.3 mm) ($P=0.02$), and there was no significant difference between the latter two.

Conclusions The thickness of the myometrium underlying the tumor on MRI was approximately one tenth of the thickness on pathology. Thus, the tumors appeared to have almost transmural invasion even when pathologically located within the superficial myometrium. This "pseudo-thinning" of the underlying myometrium and the hypointense rim on MRI could be caused by focal compression of the myometrium by the tumor, possibly due to the fragility of the myometrium at the placental site.

Keywords Uterus · Gestational trophoblastic disease · Placental site trophoblastic tumor · Multiparametric magnetic resonance imaging

✉ Takahiro Tsuboyama
ttsuboyama@gmail.com

Takuya Fukuzawa
fukuzawa.tk@gmail.com

Moto Nakaya
mnky324@gmail.com

Yasuchiyo Toyama
yasutiyo@koto.kpu-m.ac.jp

Ayumi Ohya
ayumiayu@shinshu-u.ac.jp

Katsuhiro Sano
k.sano.mg@juntendo.ac.jp

Akiko Takahata
akiko-t@koto.kpu-m.ac.jp

Kansuke Kido
k_kido@molpath.med.osaka-u.ac.jp

Noriyuki Tomiyama
tomiyama@radiol.med.osaka-u.ac.jp

[1] Kobe University, Kobe, Japan

[2] Osaka University, Osaka, Japan

[3] Shinshu University, Matsumoto, Japan

[4] Juntendo University, Tokyo, Japan

[5] Kyoto Prefectural University of Medicine, Kyoto, Japan

Published online: 21 August 2024

Introduction

Placental site trophoblastic tumor (PSTT) is a very rare form of gestational trophoblastic disease, accounting for 0.25-5% of all gestational trophoblastic neoplasms [1]. It arises from extravillous intermediate trophoblasts at the implantation site, usually after full-term pregnancy [1–3]. In contrast to other typical gestational trophoblastic neoplasms, such as invasive mole and choriocarcinoma, which are treated with chemotherapy, PSTT has unique features such as slow growth, low serum β-human chorionic gonadotropin (β-hCG) levels, and chemoresistance [1–4]. Therefore, hysterectomy is performed for PSTT [5].

No specific imaging findings have been described for PSTT, and preoperative diagnosis is often challenging [3, 6]. On ultrasonography, PSTT appears solid and cystic with variable proportions and minimal to high degree of vascularization [7]. Magnetic resonance imaging (MRI) findings have been reported in only a few cases, with PSTT showing iso-intensity to slightly hyperintensity on T2-weighted imaging (T2WI) and high intensity on diffusion-weighted imaging (DWI) [8, 9].

Accurate assessment of tumor extent is important because deep myometrial invasion, especially transmural invasion seen in approximately 30% of cases, has been described to be associated with unfavorable overall survival in PSTT [10], and the indication for fertility-sparing treatment such as uterine curettage and hysteroscopic resection may be influenced by tumor location and extent [5]. Notably, there seems to be a discrepancy between tumor location on imaging and gross appearance in previous reports, as PSTT was frequently located in the myometrium (71.4%), and only 20% of the myometrial masses protruded into the uterine cavity on ultrasound [7], whereas tumors were predominantly located in the endomyometrium and presented as polypoid or nodular masses on gross pathology [10]. We found that "pseudo-thinning" of the underlying myometrium may occur in PSTT on MRI, which may explain the discrepancy between imaging and gross appearance and also confuse the assessment of tumor extent. In this finding, the mass appeared to have almost transmural invasion on MRI, but was found to be far from the serosa on pathology.

Herein, we report multiparametric MRI findings in four cases of PSTT with special emphasis on the "pseudo-thinning" of the underlying myometrium by evaluating the discrepancies between MRI and pathology regarding the thickness of the underlying myometrium.

Materials and methods

Patients

Patients with pathologically proven PSTT from four institutions were presented at the 36th Annual Meeting of the Japanese Society of Abdominal Radiology in June 2023 and enrolled in this study. This retrospective multicenter study was approved by the institutional review boards, and the requirement for written informed consent was waived.

Image acquisition

MRI was performed with a 3T scanner (Achieva 3T X, Philips Medical Systems, Best, The Netherlands; Vantage Centurian, Canon Medical Systems, Tochigi, Japan; MAGNETOM Skyra; Siemens Healthcare, Munich, Germany) in three patients or a 1.5T scanner (Symphony, Siemens Healthcare, Erlangen, Germany) in one patient. All patients underwent T2WI, DWI, and dynamic contrast-enhanced MRI (DCE-MRI). T2WI was obtained with a two-dimensional (2D) fast spin-echo sequence (repetition time [TR], 4000–5000 ms; echo time [TE], 81–105 ms; slice thickness, 4–5 mm) in all patients, with an additional single-shot sequence (TR, 5000–21435 ms; TE, 84–102 ms; slice thickness, 5 mm) in 2 patients, and with an additional 3D sequence (TR, 1400–2400 ms; TE,102–106 ms; slice thickness, 1 mm) in 2 patients. DWI was obtained with an echo planer imaging (TR, 2293–7500 ms; TE, 55–88 ms; slice thickness, 4–5 mm; b-values, 0 and 1000 s/mm^2). An apparent diffusion coefficient (ADC) map was generated from DWI. DCE-MRI was obtained with fat-suppressed T1WI and included precontrast images and 3–6 phases of postcontrast images (45, 75, 135 s; 30, 60, 90, 120 s; 30, 70, 110 s; or 21, 42, 63, 84, 105, 126 s after injection of 0.1 mmol/kg gadolinium-based contrast agent) using a 3D gradient-echo sequence (TR, 3.1–5.9 ms; TE, 1.1–3.8 ms; slice thickness, 4–5 mm) in three patients or a 2D fast spin-echo sequence (TR, 164 ms; TE, 2.7 ms; slice thickness, 5 mm) in one patient.

Clinical analysis

Clinical findings of the patents were extracted from the medical records regarding age, obstetric history, symptoms, previous pregnancy, interval from previous pregnancy to diagnosis, and serum or urine β-hCG levels.

Image analysis

Seven radiologists (4–22 years of experience in obstetric and gynecologic MRI: median, 20 years) reviewed the MRI of

the four patients by consensus for size, tumor morphology, margins, internal texture as homogeneous or heterogeneous, signal intensity (SI), enhancement pattern, tumor location, and myometrial thickness in relation to tumor extent.

Tumor morphology was assessed for the presence or absence of solid and cystic/necrotic components, and tumor margins were classified as well-defined or ill-defined. MRI findings suggestive of partial or complete compression of the surrounding myometrium by the tumor were evaluated. These findings indicated a hypointense rim on T2WI, as seen in endometrial stromal sarcoma [11], and a hypointense rim on DCE-MRI, as seen in an enlarged uterus compressed by the sacral promontory [12].

SIs of tumors on T1WI were evaluated on precontrast imaging of DCE-MRI and defined as follows: low intensity, as SI lower than that of skeletal muscle; intermediate intensity, as SI equal to that of skeletal muscle; high intensity, as SI higher than that of skeletal muscle. Intra-tumoral hemorrhage (intra-tumoral high SI) was assessed on T1WI. SIs on T2WI were defined as follows: low intensity, as SI lower than or equal to that of skeletal muscle; moderately low intensity, as SI higher than that of skeletal muscle but lower than that of outer myometrium; intermediate intensity, as SI higher than that of outer myometrium but lower than that of endometrium; high intensity, as SI equal to or higher than that of endometrium. SIs on DWI were defined as follows: low intensity, as SI lower than or equal to that of urine; intermediate intensity, as SI higher than that of urine but lower than that of nerve root; and high intensity, as SI equal to or higher than that of nerve root. The ADC values of the tumors were measured by placing a region of interest (ROI) in the homogeneous area of the solid part of the tumors on the ADC map. The enhancement pattern was classified as early strong enhancement, i.e., enhancement as high as pelvic vascular structures in early phases (30–60 s after contrast injection), or gradual enhancement.

Regarding tumor location and extent, tumor protrusion into the uterine cavity and myometrial thickness underlying the tumor (i.e., tumor-free distance from the serosa) were evaluated on T2WI and DCE-MRI. In addition, the relationship between the tumor and the junctional zone of the uterus was evaluated on T2WI. Myometrial thickness underlying the tumor and normal myometrial thickness contralateral to the tumor were measured on the late phase images of DCE-MRI to assess focal changes in the underlying myometrium (Fig. 1).

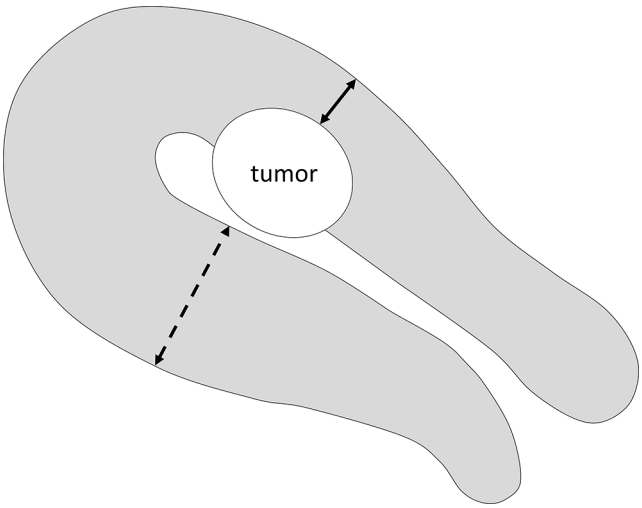

Fig. 1 Figure shows measurements of myometrial thickness underlying the tumor (double arrow) and normal myometrial thickness contralateral to the tumor (dashed double arrow) in the uterus

Pathological analysis

The pathological diagnosis of PSTT was made by experienced pathologists at each institution and confirmed by an experienced pathologist at the 36th Annual Meeting of the Japanese Society of Abdominal Radiology. All four PSTTs showed typical pathologic findings such as abundant amphophilic cytoplasm, marked nuclear atypia, and vascular invasion in the myometrium. Myometrial thickness underlying the tumor was measured on pathology.

Statistical analysis

Comparisons between normal myometrial thickness contralateral to the tumor on MRI, myometrial thickness underlying the tumor on MRI, and that on pathology were made using the Friedman test. A P value of less than 0.05 was considered significant. Statistical analysis was performed using MedCalc 22.013 (MedCalc Software, Ostend, Belgium).

Results

Clinical features

The mean age of the patients was 28.8 years (range, 26–32 years). All patients had a normal full-term pregnancy prior to manifestation of PSTT. The interval between delivery and presentation of the uterine mass was six months in three patients and seven months in one patient. All patients presented with abnormal genital bleeding. Serum β-hCG levels were elevated in three patients and normal (< 5 mIU/mL) in one. The mean serum β-hCG level at presentation was 71.9 mIU/mL (range, 1.3–154 mIU/mL). Serum or urine β-hCG levels increased in three patients and decreased in one patient prior to surgery. The clinical characteristics of each patient are listed in Table 1.

Table 1 Clinical, MRI, and pathologic features of 4 cases with placental site trophoblastic tumor

	Case 1	Case 2	Case 3	Case 4
Clinical features				
Age (years)	26	29	28	32
Obstetric history (gravida/para)	2/2	3/3	2/2	2/2
Antecedent pregnancy	Normal	Normal	Normal	Normal
Time from delivery to tumor appearance (months)	6	6	6	7
Serumβ-hCG level at presentation (mIU/ml)	154	1.3	104	28.3
Changes in preoperative serum or urine β-hCG levels	Increase	Increase	Decrease	Increase
MRI features				
Size (mm)	47.1	44.7	36.2	36.8
Morphology	Solid and cystic/necrotic	Solid and cystic/necrotic	Solid and cystic/necrotic	Solid and cystic/necrotic
Margin	Well-defined	Partly ill-defined	Well-defined	Well-defined
Tumor texture on T2WI, DWI, and DCE-MRI	Heterogeneous	Heterogeneous	Heterogeneous	Heterogeneous
Predominant signal intensity				
T1WI	Intermediate	Intermediate	Intermediate	Intermediate
T2WI	High	Low	Intermediate	Intermediate
DWI	Low	Low	Intermediate	Low
ADC value of solid components ($\times 10^{-3}$ mm^2/s)	1.4	1.5	1.3	1.1
Intra-tumoral hemorrhage	Present	Present	Present	Present
Area with early strong enhancement	Present	Present	Absent	Present
Area with gradual enhancement	Present	Present	Present	Present
Low intense rim on T2WI	Present (complete)	Present (partial)	Present (partial)	Present (complete)
Low intense rim on DCE-MRI	present (partial)	present (partial)	present (partial)	present (partial)
Protrusion into uterine cavity	Present	Present	Present	Present
Thickness of normal myometrium on MRI (mm)	13.2	9.1	10.9	9.6
Myometrial thickness underlying the tumor on MRI (mm)	1.5	0.8	1.1	1.3
Pathologic features				
Protrusion into uterine cavity	Present	Present	Present	Present
Myometrial thickness underlying the tumor on pathology (mm)	15	7.1	8	11

hCG human chorionic gonadotropin, *IU* international unit, *T2WI* T2-weighted imaging, *DWI* diffusion-weighted imaging, *DCE-MRI* dynamic contrast-enhanced magnetic resonance imaging, *T1WI* T1-weighted imaging, *ADC* apparent diffusion coefficient

MRI findings

The MRI findings of the four cases are shown in Table 1. The mean tumor diameter was 41.2 mm, ranging from 36.2 to 47.1 mm. The tumor had a well-defined margin in three patients and a partially ill-defined margin in one patient. All tumors had solid and cystic/necrotic components and showed heterogeneous SI on T1WI, T2WI, and DWI (Figs. 2, 3, 4 and 5). On T1WI, tumors predominantly showed intermediate SI, and intra-tumoral hemorrhage was seen in all tumors (Figs. 2, 3, 4 and 5). SI on T2WI was predominantly low in one patient (Fig. 3), intermediate in two patients (Figs. 4 and 5), and high in one patient (Fig. 1). In all patients, hypointense areas were seen within the tumor due to flow voids or hemorrhage. A hypointense rim between the tumor and the myometrium was seen completely in two patients (Figs. 2 and 5) and partially in two patients (Figs. 3 and 4), and the hypointense rim was continuous with the junctional zone in all patients. On DWI, the masses showed predominantly low SI in three patients (Figs. 2, 3 and 5) and intermediate SI in one patient (Fig. 4). Hyperintense areas were observed in all patients. The mean ADC value of the solid components was 1.3×10^{-3} mm^2/s (range, 1.1–1.5×10^{-3} mm^2/s). The mass had an area of early strong enhancement in three patients (Figs. 2, 3 and 5) and an area of gradual enhancement in all patients. A hypointense rim was partially present at all phases of DCE-MRI in all patients (Figs. 2, 3, 4 and 5).

Assessment of tumor location and myometrial thickness

The mass protruded into the uterine cavity on MRI and gross appearance in all patients. The thickness of the myometrium underlying the tumor on MRI was approximately one tenth of the thickness on pathology in all patients (Table 1; Figs. 2, 3, 4 and 5). The median normal myometrial thickness contralateral to the tumor on MRI, myometrial thickness underlying the tumor on MRI, and that on pathology were 10.3 mm (range, 9.1–13.2 mm), 1.2 mm (range, 0.8–1.5 mm), and 9.5 mm (range, 7–15 mm), respectively (Table 1). Myometrial thickness underlying the tumor

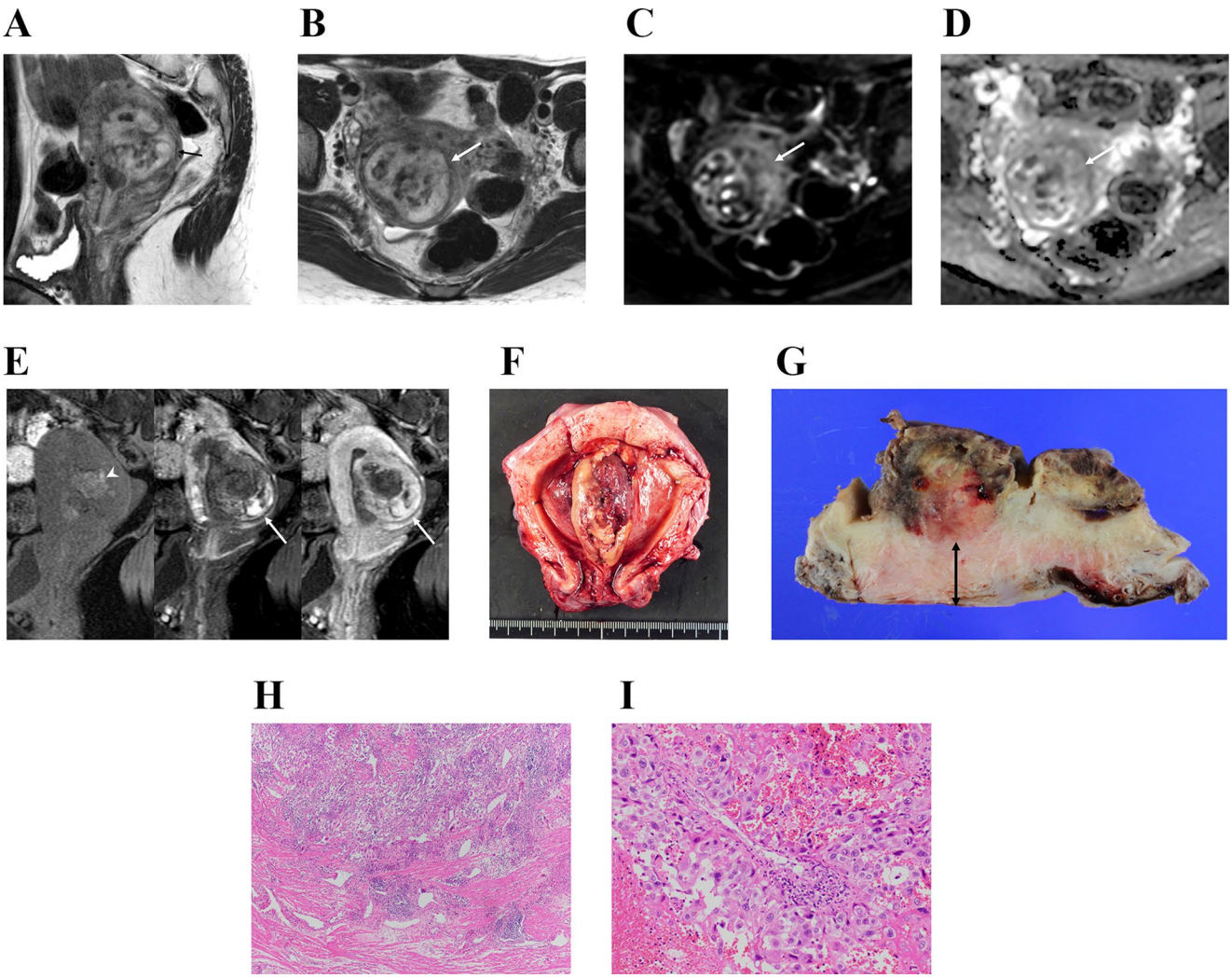

Fig. 2 Case 1: A 26-year-old female with a placental site trophoblastic tumor. **A**. Sagittal T2-weighted imaging showed a uterine mass with predominantly high signal intensity. Areas of low intensity due to hemorrhage and flow voids were present within the mass. The mass appeared to be located at the posterior wall, protruding into the uterine cavity and extending into the deep myometrium. A hypointense rim was observed that was continuous with the junctional zone (arrow). **B**. Axial T2-weighted imaging showed the hypointense rim surrounding the uterine mass (arrow). **C**. On axial diffusion-weighted imaging, the mass showed heterogeneous signal intensity from low to high. Hemorrhagic degeneration appeared to be the cause of the low and high signal intensity, whereas the solid portion showed predominantly intermediate intensity (arrow). **D**. Apparent diffusion coefficient (ADC) map showed an ADC value of 1.4×10^{-3} mm^2/s in the solid portion of the mass (arrow). **E**. Representative images of dynamic contrast-enhanced MRI (precontrast, early phase, and late phase images) are shown. Precontrast fat-suppressed T1-weighted imaging showed intra-tumoral hemorrhage with high intensity (arrowhead). Dynamic contrast-enhanced MRI showed both early strong enhancement and gradual enhancement within the mass. A hypointense rim was present on both early and late phase images (arrow). The mass appeared to invade close to the serosa (myometrial thickness underlying the tumor, 1.5 mm). **F**. Gross appearance of the resected specimen showed a polypoid mass protruding into the uterine cavity. **G**. The cut surface of the resected specimen showed that the tumor invasion front was far from the serosa (myometrial thickness underlying the tumor, 15 mm; double arrow). Intra-tumoral hemorrhage was observed. **H**. Photomicrograph (hematoxylin and eosin stain, ×40) showing infiltrative growth into the myometrium at the periphery of the tumor, with splitting of myometrial fibers. **I**. Photomicrograph (hematoxylin and eosin stain, ×200) showed characteristic vascular invasion by tumor cells

measured on MRI was significantly thinner than that measured on pathology and normal myometrial thickness contralateral to the tumor on MRI ($P=0.02$), and there was no significant difference between normal myometrial thickness contralateral to the tumor on MRI and myometrial thickness underlying the tumor on pathology.

Discussion

In our four cases of PSTT, the myometrium underlying the tumor was significantly thinner on MRI than on pathology, suggesting that it was compressed by the tumor in vivo. Furthermore, compression by the tumor occurred focally at the

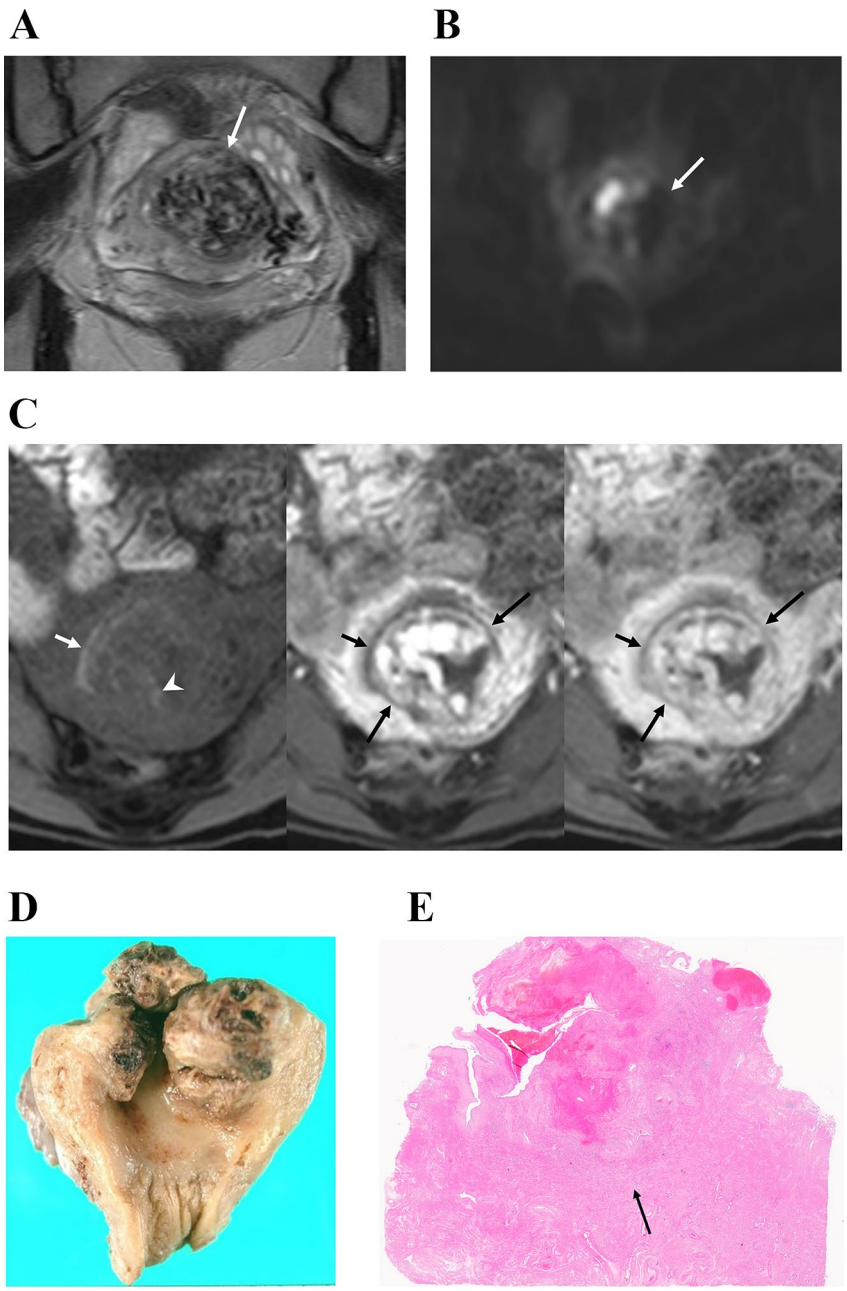

Fig. 3 Case 2: A 29-year-old female a with placental site trophoblastic tumor. **A**. Coronal T2-weighted imaging showed a polypoid uterine mass protruding into the uterine cavity. The mass showed predominantly low signal intensity due to flow voids. The mass had a hypointense rim continuous with the junctional zone (arrow). The tumor appeared to invade close to the serosa. **B**. Axial diffusion-weighted imaging showed that the mass was predominantly hypointense with high-intensity foci. The apparent diffusion coefficient value was 1.5×10^{-3} mm^2/s in the solid portion of the mass. **C**. Representative dynamic contrast-enhanced images (precontrast, early phase, and late phase images) are shown. Precontrast fat-suppressed T1-weighted imaging showed high-intensity areas within the mass (arrowhead) and uterine cavity (short arrow), suggesting intra-tumoral hemorrhage and hematometra, respectively. Dynamic contrast-enhanced MRI showed early strong enhancement associated with areas of gradual enhancement (not shown) at the tumor. A hypointense rim (long arrows) was seen that was continuous with the uterine cavity. The myometrial thickness underlying the tumor, measured on another slice, was 0.8 mm. **D**. Gross appearance of the resected specimen showed a polypoid uterine mass. **E**. Photomicrograph (hematoxylin and eosin stain, ×7) showed that the invasive tumor front (arrow) was far from the serosa. The myometrial thickness underlying the tumor was 7.1 mm. Intra-tumoral hemorrhage was present

tumor site because the normal myometrium contralateral to the tumor was significantly thicker than the myometrium underlying the tumor. This "pseudo-thinning" phenomenon is unique because myometrial compression by a polypoid tumor usually occurs diffusely throughout the myometrium.

The clinical features of our four cases were consistent with those of previously reported cases. First, PSTT usually develops after normal pregnancy with a latency of months to years, and rarely after molar pregnancy (16%) and abortion (13%) [3]. Second, the serum level of β-hCG is moderately elevated (< 1000 mIU/mL) in approximately 70% and normal (< 5 mIU/mL) in approximately 10% of PSTT [4].

All four tumors showed heterogeneous SI on T1WI, T2WI, and DWI. On T1WI, all tumors had an area of high SI due to hemorrhage. The SIs of the tumors on T2WI were quite different among the four cases, probably because of the different amount of tumor cells, necrosis, hemorrhage, and extracellular eosinophilic fibrinoid material within the four tumors [2]. The tumors predominantly showed low to intermediate SI on DWI and relatively high ADC values, in contrast to a reported case of PSTT and other common malignant tumors showing high SI on DWI and low ADC values [9]. The cellularity of our four cases of PSTT seems to be not so high due to the admixture of hemorrhage, necrosis, and fibrinoid material. The reported case of PSTT with

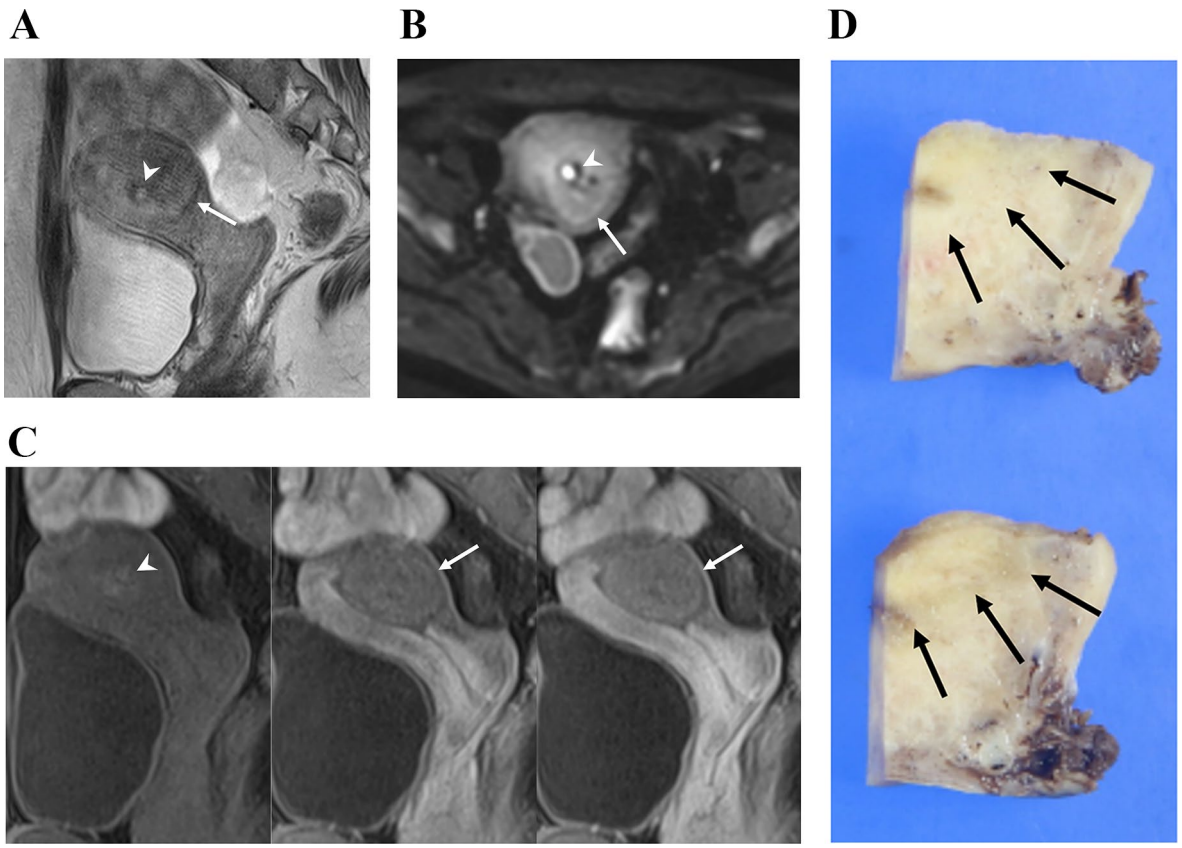

Fig. 4 Case 3: A 28-year-old female with a placental site trophoblastic tumor. **A**. Sagittal T2-weighted imaging showed a uterine mass with intermediate signal intensity. The mass contained a cystic or hemorrhagic component (arrowhead). There was a hypointense rim (arrow). **B**. On axial diffusion-weighted imaging, the mass showed intermediate signal intensity (arrow). Intra-tumoral hemorrhage showed high signal intensity (arrowhead). The solid portion of the mass had an apparent diffusion coefficient value of 1.3×10^{-3} mm^2/s. **C**. Representative dynamic contrast-enhanced images (precontrast, early phase, and late phase images) are shown. Precontrast fat-suppressed T1-weighted imaging showed an area of high intensity within the mass, consistent with intra-tumoral hemorrhage (arrowhead). On dynamic contrast-enhanced MRI, the mass showed gradual enhancement. A hypointense rim was present (arrow), and the myometrial thickness underlying the tumor was 1.1 mm. **E**. The cut surface of the resected specimen showed that the mass was predominantly in the myometrium, but the invasion front (arrows) was 8 mm apart from the serosa

high SI on DWI invaded almost the entire myometrium and might be more aggressive than our cases [9]. Foci of high SI on DWI were found in all cases, possibly due to hemorrhage or areas of high cellularity. Consistent with previous reports, our four cases showed different enhancement patterns [7, 8]. Hypervascular structures, typical of many other gestational trophoblastic diseases [3], were present in three of four tumors that had increased serum or urine β-hCG levels prior to surgery, and the other tumor had minimal enhancement associated with decreased β-hCG levels prior to surgery. Therefore, the vascularity of the tumor may be correlated with the β-hCG level, as previously reported [13]. According to our results, PSTTs showed various and nonspecific MRI findings, and thus, accurate diagnosis by MRI may be difficult.

We found that PSTT could cause focal compression of the underlying myometrium, resulting in some notable imaging findings. First, the tumors showed well-defined margins with hypointense rim on T2WI and DCE-MRI despite infiltrative tumor growth pathologically. The compressed myometrium may be responsible for the hypointense rim on T2WI and DCE-MRI. Interestingly, it has been reported that low-grade endometrial stromal sarcoma, which is also characterized by slow growth, has a low intense rim on T2WI while tumor cells infiltrate the myometrium with a tongue-like pattern pathologically [11]. Hypointense rim on DCE-MRI in PSTT resembles pseudocapsules of renal cell carcinoma, but the former showed hypointensity in all phases of DCE-MRI, while the latter shows hypointensity in early phase and hyperintensity in late phase [14]. This difference may be caused by the different pathological features, because the pseudocapsule of renal cell carcinoma contains fibrous component, but PSTTs does not. Another possible cause of the hypointense rim on T2WI is the displaced junctional zone, because the hypointense rim was continuous with the junctional zone. Brandt et al. reported that 2 cases

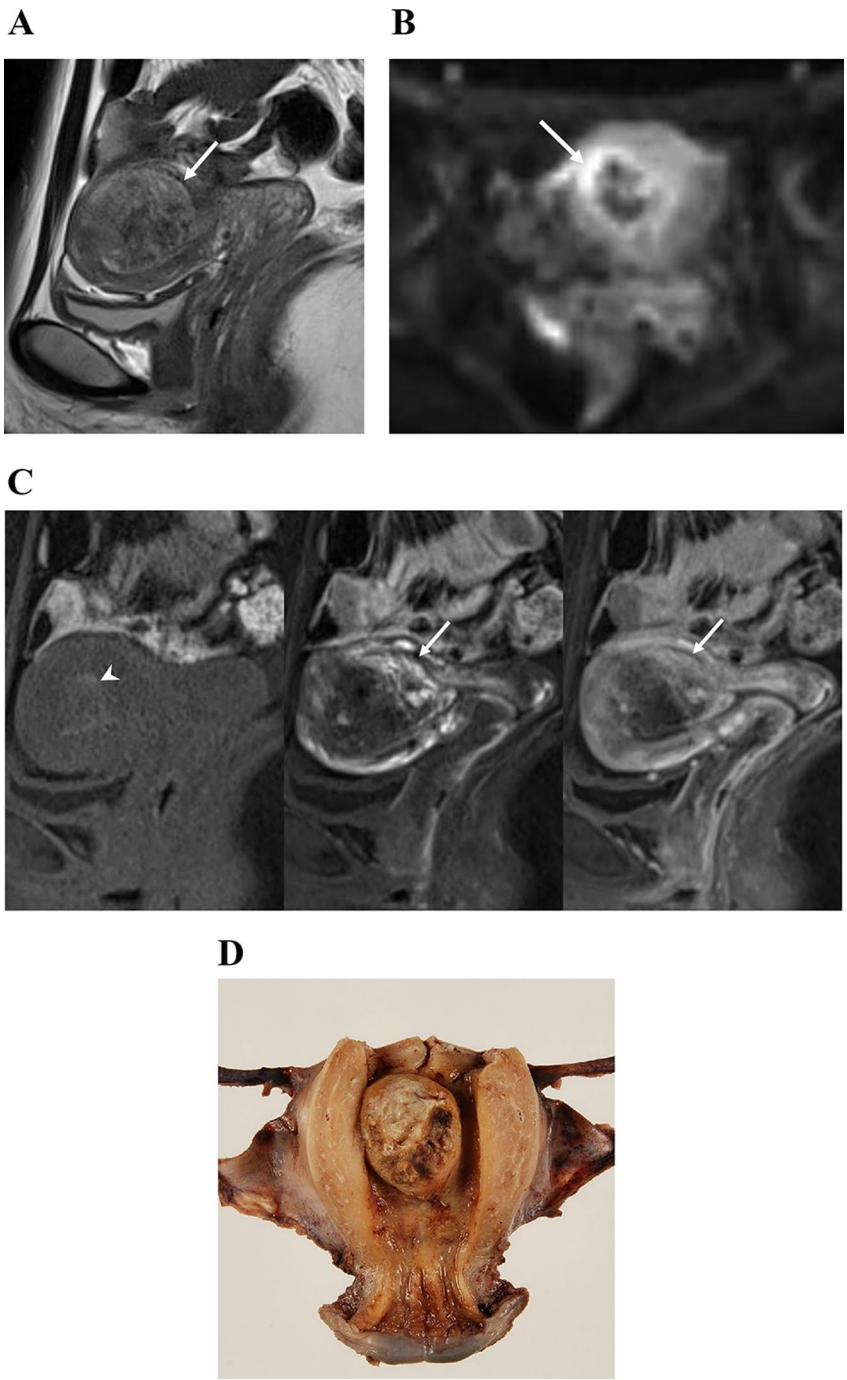

Fig. 5 Case 4: A 32-year-old female with a placental site trophoblastic tumor. **A**. Sagittal T2-weighted imaging showed a polypoid uterine mass with heterogeneous signal intensity. A hypointense rim (arrow) was present and continuous with the junctional zone. The mass extended close to the serosa of the posterior wall. **B**. Axial diffusion-weighted imaging showed that the mass was predominantly hypointense with some hyperintense areas (arrow). The solid portion of the mass had an apparent diffusion coefficient value of 1.1×10^{-3} mm^2/s. **C**. Representative dynamic contrast-enhanced images (precontrast, early phase, and late phase images) are shown. Precontrast fat-suppressed T1-weighted imaging showed high intensity within the mass, suggesting intratumoral hemorrhage (arrowhead). On dynamic contrast-enhanced MRI, the mass had an area of early strong enhancement and an area of gradual enhancement. A hypointense rim was present (arrow), and the myometrial thickness underlying the tumor was 1.3 mm. **D**. Gross appearance of the resected specimen showed a polypoid mass. The myometrial thickness underlying the tumor was 11 mm pathologically

of small PSTT (1.5 cm) were located in the inner myometrium and displaced the junctional zone on T2WI [8]. Since PSTT originates from extravillous trophoblasts infiltrating the myometrium [2], it is likely that PSTT often develops within the junctional zone and displaces the junctional zone.

Second, pseudo-thinning of the myometrium underlying the tumor may also be caused by the focal compression of the tumor. The myometrium at the tumor site may be focally softened by tumor invasion. Another possible reason for the focal change of the myometrium underlying the tumor may be the pathophysiological change similar to subinvolution of the placental site [15]. During pregnancy, extravillous trophoblasts infiltrate the decidua, myometrium, and spiral arteries of the placental site. The spiral arteries then lose endothelial and smooth muscle cells and become distended [2, 15]. Subinvolution of the placental bed vessels represents a condition in which regression of the remodeled vasculature occurs at all sites except the placental bed, where there is an apparent failure of physiological obliteration of the large vessels underlying the placental site [15]. At the

tumor site of PSTT, vascular invasion by the tumor similar to that of extravillous trophoblasts remains after delivery, and the soft myometrium may occur as seen in the subinvolution of the placental site.

Pseudo-thinning of the underlying myometrium on MRI may lead to misinterpretation of tumor extent because tumors appear to have almost transmural invasion on MRI but do not actually have transmural invasion on pathology. Therefore, knowledge of this phenomenon in combination with MRI findings suggesting focal compression of the underlying myometrium may help avoid misdiagnosis of transmural tumor invasion on MRI.

The differential diagnosis of PSTT includes other types of gestational trophoblastic neoplasms, exaggerated placental site reaction, and retained products of conception (RPOC). As discussed above, the role of imaging in the differential diagnosis is limited and clinical features and biopsy play the major role. Serum β-hCG levels are useful in differentiating PSTT from choriocarcinoma and invasive mole, as the latter are associated with extremely high levels of β-hCG (> 100000–1000000 mIU/mL) [16]. Epithelioid trophoblastic tumor (ETT) is a rare form of gestational trophoblastic neoplasm arising from chorionic-type intermediate trophoblasts [1]. ETT shares many similarities with PSTT in that ETT develops after normal pregnancy, is associated with mildly elevated serum β-hCG (< 2500mIU/mL), and is chemoresistant [1–3, 5, 16]. Because ETT shows expansile growth in contrast to the infiltrative growth of PSTT, it has been reported that a well-demarcated border with peripheral Doppler signal on ultrasound is more suggestive of ETT than PSTT [17]. However, this sonographic differentiation method may not be applicable to MRI, because PSTT in our study often had well-defined borders on MRI despite the infiltrative growth of the tumor due to focal myometrial compression. From a clinical point of view, both ETT and PSTT require hysterectomy rather than chemotherapy, and the differentiation between ETT and PSTT does not seem to be critical [5]. Exaggerated placental site reaction is pathologically similar to PSTT, but it is a physiological process rather than a true neoplasm and does not manifest as macroscopic lesions [1]. When exaggerated placental site reaction forms a macroscopic mass, differentiation from PSTT is quite difficult [18]. RPOC initially consists of retained villi and then undergoes necrosis with fibrin deposition, resulting in a pathological condition called placental polyps [19, 20]. RPOC most commonly develops after medical abortion (up to 15%), followed by miscarriage or first or second trimester abortion (6%) and term delivery (1%) [19]. RPOC shows varying degrees of vascularization from none to marked on ultrasound and MRI and heterogeneous SIs on T1WI and T2WI [21, 22]. Serum β-hCG levels are slightly elevated, especially after miscarriage, and β-hCG is elevated in only 9% of patients after delivery [23]. Unlike PSTT, RPOC does not invade the myometrium and may show spontaneous regression within a few months [20].

In conclusion, this case series of PSTT showed that pseudo-thinning of the underlying myometrium may occur on MRI, possibly due to focal compression by the polypoid tumor, and thus tumor extent may be carefully assessed to avoid overdiagnosis of myometrial invasion.

Author contributions TT was involved in the study design, acquisition of data, analysis and interpretation of data, and drafting of the manuscript. TF, MN, YT, AO, KS, and AT were involved in the data collection, interpretation of data, and drafting of the manuscript. KK was involved in the interpretation of data. NT was involved in the analysis and interpretation of data and drafting themanuscript. All authors reviewed the manuscript.

Funding No funding was received for this study.

Data availability No datasets were generated or analysed during the current study.

Declarations

Ethical approval This study was conducted in accordance with the principles of the Declaration of Helsinki. This study was approved by the Research Ethics Committee of Osaka University (approval number: 23216).

Informed consent Written informed consent for participation was waived owing to the retrospective nature of the study, and patient records were anonymously analyzed.

Competing interests The authors declare no competing interests.

References

1. Baergen RN, Cheung AN, Hui P, Kaur B, Mao TL (2020) Placental site trophoblastic tumour. In: WHO Classification of Female Genital Tumors. 5th ed. IARC, Lyon.
2. Shih IM, Kurman RJ (2001) The pathology of intermediate trophoblastic tumors and tumor-like lesions. Int J Gynecol Pathol 20:31–47. https://doi.org/10.1097/00004347-200101000-00004
3. Chawla T, Bouchard-Fortier G, Turashvili G, et al (2023) Gestational trophoblastic disease: an update. Abdom Radiol (NY) 48:1793–1815. https://doi.org/10.1007/s00261-023-03820-5
4. Liu W, Zhao W, Huang X (2022) Outcomes and prognostic factors of placental-site trophoblastic tumor: a retrospective study of 58 cases. Arch Gynecol Obstet 306:1633–1641. https://doi.org/10.1007/s00404-022-06502-7
5. Ngan HYS, Seckl MJ, Berkowitz RS, et al (2021) Diagnosis and management of gestational trophoblastic disease: 2021 update. Int J Gynaecol Obstet 155 (Suppl 1):86–93. https://doi.org/10.1002/ijgo.13877
6. Moutte A, Doret M, Hajri T, et al (2013) Placental site and epithelioid trophoblastic tumours: diagnostic pitfalls. Gynecol Oncol128:568–572. https://doi.org/10.1016/j.ygyno.2012.11.010
7. Zhou Y, Lu H, Yu C, Tian Q, Lu W (2013) Sonographic characteristics of placental site trophoblastic tumor: Placental site

trophoblastic tumor. Ultrasound Obstet Gynecol 41:679–684. https://doi.org/10.1002/uog.12269
8. Brandt KR, Coakley KJ (1998) MR appearance of placental site trophoblastic tumor: a report of three cases. Am J Roentgenol 170:485–487. https://doi.org/10.2214/ajr.170.2.9456970
9. Lucas R, Cunha TM, Santos FB (2015) Placental site trophoblastic tumor: a case report and review of the literature. J Radiol Case Rep 9:14–22. https://doi.org/10.3941/jrcr.v9i4.2146
10. Baergen RN, Rutgers JL, Young RH, Osann K, Scully RE (2006) Placental site trophoblastic tumor: A study of 55 cases and review of the literature emphasizing factors of prognostic significance. Gynecol Oncol 100:511–520. https://doi.org/10.1016/j.ygyno.2005.08.058
11. Furukawa R, Akahane M, Yamada H, et al (2010) Endometrial stromal sarcoma located in the myometrium with a low-intensity rim on T2-weighted images: report of three cases and literature review. J Magn Reson Imaging 31:975–979. https://doi.org/10.1002/jmri.22126
12. Uotani K, Monzawa S, Adachi S, et al (2007) Hypointensity on postcontrast MR imaging from compression of the sacral promontory in enlarged uterus with huge leiomyoma and adenomyosis. Magn Reson Med Sci 6:61–66. https://doi.org/10.2463/mrms.6.61.
13. Yamashita Y, Torashima M, Takahashi M, et al (1995) Contrast-enhanced dynamic MR imaging of postmolar gestational trophoblastic disease. Acta Radiol 36:188–192.
14. Ogawa Y, Morita S, Takagi T, et al (2021) Early dark cortical band sign on CT for differentiating clear cell renal cell carcinoma from fat poor angiomyolipoma and detecting peritumoral pseudocapsule. Eur Radiol 31:5990–5997. https://doi.org/10.1007/s00330-021-07717-z
15. Andrew AC, Bulmer JN, Wells M, Morrison L, Buckley CH (1989) Subinvolution of the uteroplacental arteries in the human placental bed. Histopathology 15:395–405. https://doi.org/10.1111/j.1365-2559.1989.tb01591.x
16. Silva ALMD, Monteiro KDN, Sun SY, Borbely AU (2021) Gestational trophoblastic neoplasia: Novelties and challenges. Placenta 116:38–42. https://doi.org/10.1016/j.placenta.2021.02.013
17. Qin J, Ying W, Cheng X, et al (2014) A well-circumscribed border with peripheral Doppler signal in sonographic image distinguishes epithelioid trophoblastic tumor from other gestational trophoblastic neoplasms. PLoS One 9:e112618. https://doi.org/10.1371/journal.pone.0112618
18. Yeasmin S, Nakayama K, Katagiri A, et al (2010) Exaggerated placental site mimicking placental site trophoblastic tumor: case report and literature review. Eur J Gynaecol Oncol 31:586–589.
19. Foreste V, Gallo A, Manzi A, et al (2021) Hysteroscopy and Retained Products of Conception: An Update. Gynecol Minim Invasive Ther 10:203–209. https://doi.org/10.4103/GMIT.GMIT_125_20
20. Shiina Y, Itagaki T, Ohtake H (2018) Hypervascular retained product of conception: Characteristic magnetic resonance imaging and possible relationship to placental polyp and pseudoaneurysm. J Obstet Gynaecol Res 44:165–170. https://doi.org/10.1111/jog.13481
21. Iraha Y, Okada M, Toguchi M, et al (2018) Multimodality imaging in secondary postpartum or postabortion hemorrhage: retained products of conception and related conditions. Jpn J Radiol 36:12–22. https://doi.org/10.1007/s11604-017-0687-y
22. Noonan JB, Coakley FV, Qayyum A, et al (2003) MR imaging of retained products of conception. AJR Am J Roentgenol 181:435–439. https://doi.org/10.2214/ajr.181.2.1810435
23. Smorgick N, Segal H, Eisenberg N, et al (2022) Serum β-HCG level in women diagnosed as having retained products of conception: A prospective cohort study. J Minim Invasive Gynecol 29:424–428. https://doi.org/10.1016/j.jmig.2021.11.006